Single-Walled Carbon Nanotubes

From Fundamental Studies to New Device Concepts

TERI WANG ODOM, JIN-LIN HUANG, AND CHARLES M. LIEBER

Department of Chemistry and Chemical Biology, Harvard University, Cambridge, Massachusetts 02138, USA

ABSTRACT: Single-walled carbon nanotubes (SWNTs) are ideal systems for investigating fundamental properties in one-dimensional electronic systems and have the potential to revolutionize many aspects of nano/molecular electronics. Scanning tunneling microscopy (STM) has been used to characterize the atomic structure and tunneling density of states of individual SWNTs. Detailed spectroscopic measurements showed one-dimensional singularities in the SWNT density of states for both metallic and semiconducting nanotubes. The results obtained were compared to and agree well with theoretical predictions and tight-binding calculations. SWNTs were also shortened using the STM to explore the role of finite size, which might be exploited for device applications. Segments less than 10 nm exhibited discrete peaks in their tunneling spectra, which correspond to quantized energy levels, and whose spacing scales inversely with length. Finally, the interaction between magnetic impurities and electrons confined to one dimension was studied by spatially resolving the local electronic density of states of small cobalt clusters on metallic SWNTs. Spectroscopic measurements performed on and near these clusters exhibited a narrow peak near the Fermi level that has been identified as a Kondo resonance. In addition, spectroscopic studies of ultrasmall magnetic nanostructures, consisting of small cobalt clusters on short nanotube pieces, exhibited features characteristic of the bulk Kondo resonance, but also new features due to their finite size.

KEYWORDS: single-walled carbon nanotubes; scanning tunneling microscopy; one-dimensional system; finite-size effects; magnetic impurities; Kondo effect

INTRODUCTION

One-dimensional (1D) nanostructures, such as carbon nanotubes and nanowires, are poised to become important building blocks for molecule-based, electrical circuits. These materials not only offer the potential to serve as interconnects between active molecular elements in a device but also have the ability to function as the device element itself.[1] Recent demonstrations of the latter include using semiconduct-

Address for correspondence: Teri Wang Odom, Harvard University, Department of Chemistry, 12 Oxford Street, Box 328, Cambridge, MA 02138. Voice: 617-495-9436; fax: 617-495-2500.
todom@fas.harvard.edu

Ann. N.Y. Acad. Sci. 960: 203–215 (2002).

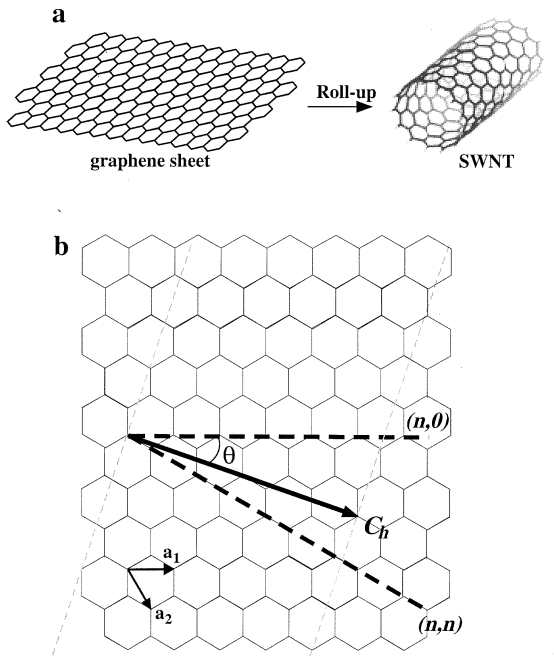

FIGURE 1. **(a)** Schematic of a portion of a graphene sheet rolled up to form a SWNT. **(b)** 2D graphene sheet illustrating lattice vectors $\mathbf{a}_1$ and $\mathbf{a}_2$, and the roll-up vector $\mathbf{C}_h = n\mathbf{a}_1 + m\mathbf{a}_2$. The achiral, limiting cases of $(n, 0)$ and (n, n) armchair are indicated with *thick*, *dashed lines*, and the chiral θ angle is measured from the zigzag direction. The *light*, *dashed parallel lines* define the unrolled, infinite SWNT. The diagram has been constructed for $(n, m) = (4, 2)$.

ing carbon nanotubes in field-effect transistors[2,3] and doped semiconducting nanowires in nanoscale optoelectronic and other electrical devices.[4,5]

In order to exploit the unique physical properties of these 1D materials for technological applications, it is important to characterize in detail their intrinsic properties. Determination of the properties of individual nanostructures has both great scientific and practical value. Namely, nanostructures prepared by either synthetic or fabricated approaches are not identical objects and typically exhibit dispersions in both size and structure. Hence, the characterization of individual structures is crucial to realize the potential and assess the limitations of employing these materials in molecular devices.[6,7] To this end, we will discuss scanning tunneling microscopy (STM) experiments that elucidate the electronic properties of single-walled carbon nanotubes (SWNTs).

A SWNT can be viewed as a strip cut from an infinite graphene sheet that is rolled up seamlessly to form a tube (FIG. 1a). The diameter and helicity of a SWNT are defined by the roll-up vector $\mathbf{C}_h = n\mathbf{a}_1 + m\mathbf{a}_2 \equiv (n, m)$, which connects crystallographically equivalent sites on this sheet. $\mathbf{a}_1$ and $\mathbf{a}_2$ are the graphene lattice vectors, and n and m are integers. Electronic-band structure calculations predict that the (n, m) in-

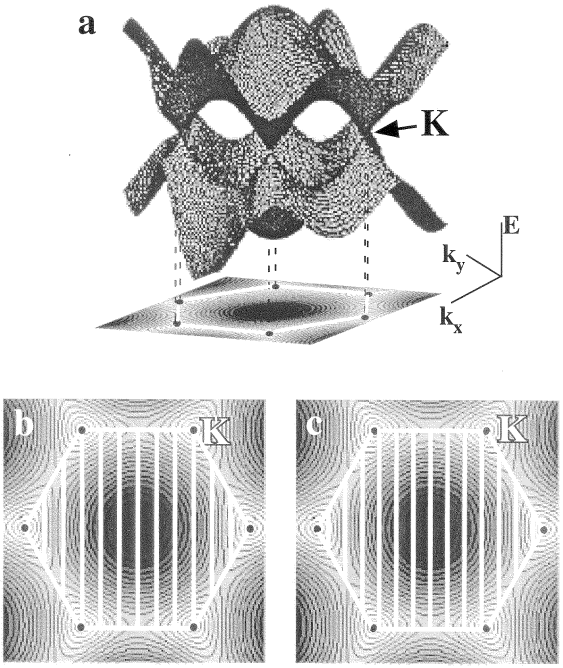

FIGURE 2. **(a)** Three-dimensional view of the graphene π/π^* bands and its 2D projection. The *white hexagon* defines the first Brilluoin zone of graphene, and the *black dots* in the corners are the graphene **K** points. **(b)** Example of the allowed subbands for a metallic tube. Schematic depicts (9, 0). **(c)** Example of the quantized subbands for a semiconducting tube. Schematic depicts (10, 0).

dices determine whether a SWNT will be a metal or a semiconductor.[8–10] To understand this ability to exhibit distinct electronic properties within an all-carbon, sp^2-hybridized network, it is instructive to consider the electronic properties of graphite.

Graphite is a semimetal or zero-gap semiconductor whose valence and conduction bands touch and are degenerate at six **K** (k_F) points (FIG. 2a). As a finite piece of the 2D graphene sheet is rolled up to form a 1D tube, the periodic boundary conditions imposed by $\mathbf{C}_h$ can be used to enumerate the allowed 1D subbands, the quantized states resulting from radial confinement. If one of these subbands passes through one of the **K** points, the nanotube will be metallic, otherwise it will be semiconducting (FIG. 2b). SWNTs are metallic if their (n, m) indices satisfy the condition in which $(n - m)/3$ is an integer; otherwise, the SWNTs are semiconducting.[8–10] Based solely on geometry, one-third of the nanotubes will be metallic and two-thirds semiconducting.

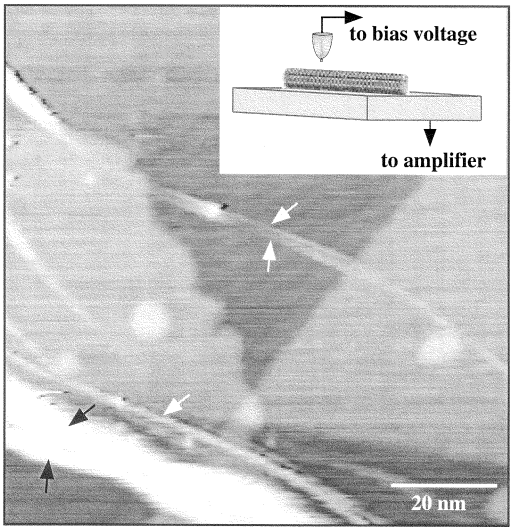

FIGURE 3. Large-area STM image showing several small ropes and isolated SWNTs on a stepped Au(111) surface. The *white arrow* indicates individual SWNTs and the *black arrows* point to small ropes of SWNTs. *Inset*: Schematic diagram of the STM experiment. (Adapted from Hu *et al.*[7])

ATOMIC STRUCTURE AND ELECTRONIC PROPERTIES OF SWNTS

Scanning tunneling microscopy and spectroscopy (STS) offer the potential to probe whether structural changes in SWNT geometry produce distinct electronic properties, since these techniques are capable of simultaneously resolving the atomic structure and electronic density of states (DOS) of a material. We have carried out STM measurements in ultrahigh vacuum on SWNT samples grown by laser vaporization.[11] This method produces a mixture of individual tubes and ropes, superstructures of single nanotubes packed together hexagonally. Such size dispersions in SWNT samples are readily observed in large-scale STM images (FIG. 3).

Atomically resolved STM images of SWNTS reveal significant structural variety among nanotubes (FIG. 4). The measured chiral angle and diameter of the tube in FIGURE 4a constrain the (n, m) indices to either (11, 2) or (12, 2). Note that an (11, 2) tube is expected to be metallic, whereas a (12, 2) tube should be semiconducting [i.e., $(n - m)/3$ is not an integer]. On the other hand, the chiral angle and diameter of the SWNT in FIGURE 4b constrain the indices to (14, −3). This tube has chirality opposite the SWNT in FIGURE 4a. To investigate whether their electronic properties depend on structure, we performed tunneling spectroscopy measurements on these tubes. Specifically, tunneling current I versus voltage V data was measured at specific sites along the tubes and differentiated to yield the normalized conductance, $(V/I)dI/dV$, which provides a good measure of the local density of electronic states (LDOS).

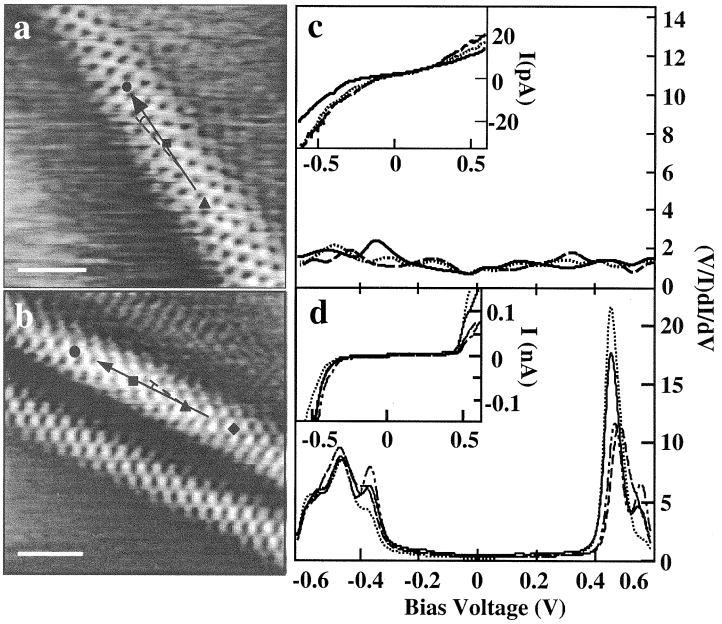

FIGURE 4. (a,b) Constant-current images of SWNTs recorded with bias voltages of 50 and 300 mV, respectively. The *solid arrow* highlights the tube axis, and the *dashed line* indicates the zigzag direction. The symbols correspond to positions where *I–V* curves were recorded. **(c,d)** Calculated normalized conductance (*V*/*I*)*dI*/*dV* and measured *I–V* (*inset*) recorded at the sites indicated by the symbols in parts **(a)** and **(b)**. (Adapted from Odom *et al.*[16])

I–V data recorded along the two tubes discussed earlier exhibit very different features (FIG. 4c, 4d), and the corresponding LDOS are quite distinct. For the tube we assigned as (11, 2) or (12, 2), the LDOS is finite and constant between −0.6 and +0.6 V. This behavior is characteristic of a metal, and thus shows that the (11, 2) indices provide the best description for the tube. In contrast, the normalized conductance data determined for the (14, −3) tube exhibit an absence of electronic states at low energies but the presence of sharp peaks at −0.325 and +0.425 V, which correspond to the conduction and valence bands of the semiconducting tube. These key measurements first verified the unique ability of SWNTs to exhibit fundamentally different electronic properties with only subtle variations in structure.[12,13]

ONE-DIMENSIONAL BAND STRUCTURE OF SWNTS

The characterization of semiconducting and metallic SWNTs with subtle changes in structure confirms the remarkable electronic behavior of carbon nanotubes, and we believe represents a significant step forward in understanding these 1D materials. Another characteristic signature of a 1D system is the divergent van Hove singularities (VHS), manifest as peaks, in its DOS. We have already observed evidence of

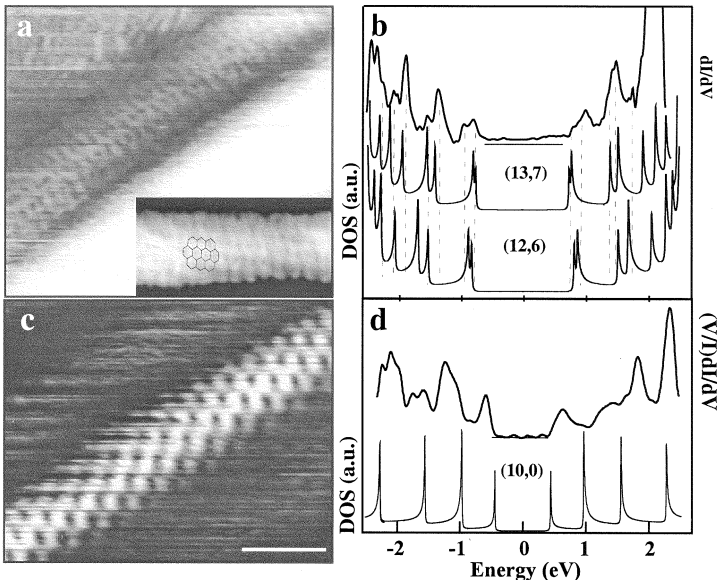

FIGURE 5. **(a)** STM image of a small SWNT rope. Tunneling spectra were recorded on the isolated upper tube. The *inset* shows an atomic-resolution image of the tube, and a portion of a hexagonal lattice is overlaid to guide the eye. **(b)** Comparison of the DOS obtained from experiment (*upper curve*) and a π-only tight-binding calculation for the (13, 7) SWNT. The calculated DOS for a (12, 6) tube is included for comparison. **(c)** STM image of a SWNT on the surface of a rope. **(d)** Comparison of the DOS obtained from experiment (*upper curve*) and calculation for the (10, 0) SWNT (*lower curve*). (Adapted from Odom *et al.*[16])

these peaks in the DOS of semiconducting SWNTs. By recording *I–V* data over a larger voltage range, however, we should be able to observe a series of singularities that are distinct for either metallic or semiconducting SWNTs. Moreover, when spectroscopic measurements are made on atomically resolved nanotubes, it is possible to compare quantitatively the experimental DOS with the calculated DOS for specific (*n*, *m*) indices.

An STM image of several SWNTs is shown in FIGURE 5a. We have performed spectroscopic measurements on the upper tube, whose indices we assigned as (13, 7). The *dI/dV* recorded on this tube can be broadly separated into two regions: (1) near the Fermi energy, E_F, the DOS is finite and constant, and (2) away from E_F, the DOS exhibits a series of sharp peaks that correspond to extremal points in the 1D energy bands. We have made a direct comparison of these experimental data to the theoretical electronic band structure calculated using a π-only tight-binding model.[14] Our spectroscopic data show good agreement with the calculated DOS for the (13, 7) tube, especially below E_F, where the first seven peaks correspond well (FIG. 5b). Above E_F, some deviation between the experimental data and calculations exists. The observed differences may be due to band repulsion, which arises from curvature-induced hybridization.[15] We have also investigated the sensitivity of the VHS to variations in the (*n*, *m*) indices by calculating the DOS of the next closest

metallic SWNT; that is, a (12, 6) tube. It is worth noting that the poor agreement in this case demonstrates that small variations in diameter and helicity do produce experimentally distinguishable changes in the DOS.

We have also characterized spectroscopically a small-diameter semiconducting nanotube (FIG. 5c) whose indices are (10, 0).[16] Sharp peaks are also observed in the normalized conductance of this nanotube tube away from E_F; however, unlike the metallic (13, 7) tube above, near the Fermi level, there is an absence of electronic states. Similar to the preceding comparison, the experimental DOS exhibits relatively good agreement with the calculated (10, 0) DOS below E_F, but poorer agreement above (FIG. 5d). Nevertheless, these results show clearly that the VHS spikes in the electronic-band structure, which are characteristic of 1D systems, can be measured experimentally and agree well with the DOS calculated using π-only tight-binding models.

FINITE-SIZED EFFECTS IN SWNTS

Up until this point, we have focused our studies on SWNTs that have retained features of a periodic 1D system. As the length of a SWNT is reduced, one ultimately will reach the limit of a fullerene molecular cluster—a 0D object. In this regard, studies of finite-sized SWNTs offer a unique opportunity to probe the connection between and evolution of electronic structure in periodic molecular systems. Investigations of finite-sized effects in SWNTs are also important to the future utilization of nanotubes in device applications. Low-temperature transport experiments on metallic SWNTs have shown that μm-long tubes behave as Coulomb islands in single electron transistors, with an island energy level spacing ΔE characteristic of 1D particle-in-a-box states.[17,18] Because the Coulomb charging energy $E_c \propto 1/L$ (L is the nanotube length), shorter nanotubes allow the working temperature of such devices to increase. In addition, finite-sized effects should be visible at room temperature if $\Delta E > k_B T$; thus a resonant tunneling device may be conceived with nanotubes whose lengths are less than 50 nm.

There are several approaches to fabricating short SWNT pieces.[19,20] We have found that by creating them *in situ*, that is, by using voltage pulses from the STM tip to cut nanotubes into desired fragment lengths,[16] we are able to probe length effects within the same tube. STM images of nanotubes shortened to six and five nanometers, respectively, are shown in FIGURE 6a and 6b. Spectroscopic measurements performed along the shortened tubes reveal sharp, equally spaced peaks at low energies in the $(V/I)dI/dV$. Because the DOS of bulk metallic SWNTs is constant at low energies until the first band edges (ca. ±1 eV), we can attribute these peaks to resonant electron tunneling through discrete energy levels due to the finite length of the SWNTs. We also compared this peak spacing directly with a 1D particle-in-a-box model, where the energy level spacing is 1.67 eV/L (nm).[18] The 6-nm-long tube (FIG. 6a) exhibits an approximate peak spacing of 0.27 eV. Within this 1D box model, a 6-nm tube has an average level spacing ΔE = 1.67 eV/6 = 0.28 eV, which is in reasonable agreement with the experimental results. For the latter tube with its shorter length, the observed peak spacing is also wider, as expected from this model.

We have also studied the effects of finite length on semiconducting nanotubes. An STM image of an atomically resolved 20-nm SWNT that has also been characterized

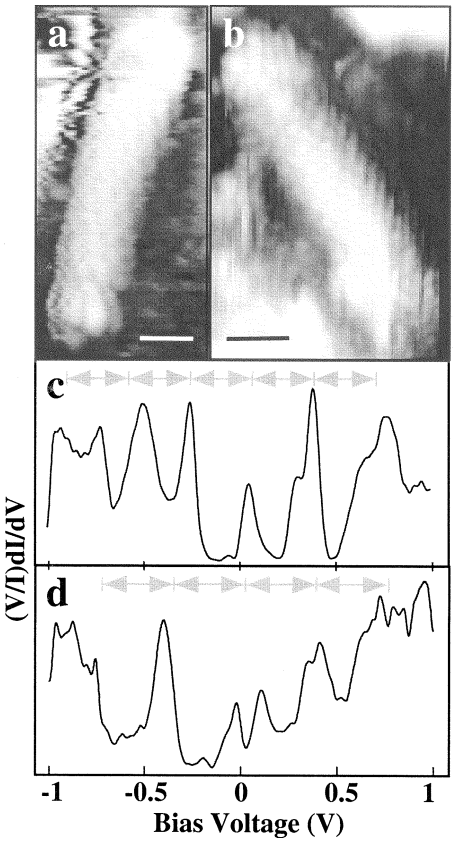

FIGURE 6. (a,b) STM images of SWNTs cut by voltage pulses and shortened into lengths of 6 nm and 5 nm, respectively. *Scale bar* is 1 nm. **(c,d)** Averaged normalized conductance from the nanotubes in **(a,b)**, respectively. The *gray arrows* indicate a near-equidistant peak-splitting characteristic of the discrete energy-level spacing.

spectroscopically before shortening is shown in FIGURE 7a. The bright, open ends of this SWNT reflect the increased localized electron density due to dangling carbon bonds created as a result of cutting in vacuum. Noticeably, the tunneling spectroscopy obtained from the center of the shortened tube shows a striking resemblance to the spectrum observed before cutting (FIG. 7b); namely, the positions of the VHS are nearly identical. It thus appears that a 20-nm semiconducting tube fragment exhibits bulklike behavior. We have found that even down to 5-nm tube lengths (FIG. 7c), semiconducting fragments show bulklike electronic behavior (FIG.7d). Hence it appears that to exploit the potential properties of finite-sized semiconducting nanotubes for device applications, the lengths need to be reduced to less than 5 nm.

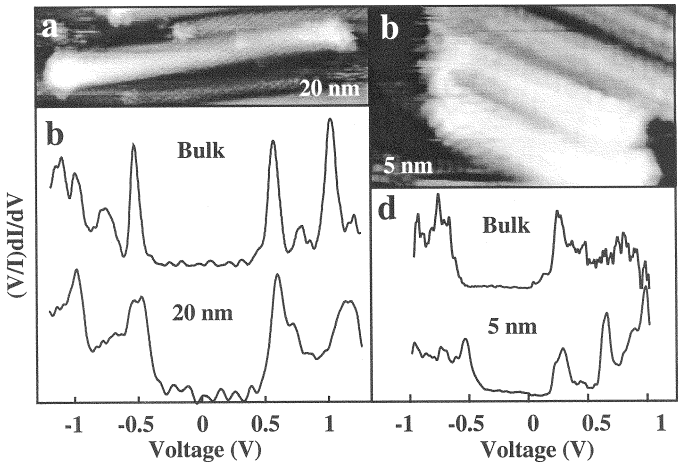

FIGURE 7. **(a)** STM image of a SWNT shortened to 20 nm. **(b)** Comparison of the normalized conductance for the tube in part **(a)** and the uncut tube before cutting. The spectra are nearly identical. **(c)** STM image of a SWNT shortened to 5 nm. **(d)** Comparison of the normalized conductance for the tube in part (c) and the uncut tube before cutting.

MAGNETIC IMPURITY EFFECTS ON SWNTS

The final experiment we will describe, the effect of magnetic impurities on the electronic structure of SWNTs, is important for a number of reasons. First, the study reconfirms all the STM results on ideal carbon nanotubes to date. Second, it offers the opportunity to study the effect of magnetic impurities on a 1D system. Third, it addresses an important question about the robustness of the intrinsic properties of nanostructures in the presence of impurities. Finally, the experiment demonstrates how systems with well-characterized impurities may exhibit novel properties that may hold promise for future applications.

A natural extension of our STM studies of SWNTs would be to introduce perturbations to the nanotube system. We chose to decorate the nanotubes with magnetic impurities, motivated by the lack of understanding between such impurities and low-dimensional electron systems. The interaction between the magnetic moment of a magnetic impurity atom and the conduction electron spins of a nonmagnetic host, the Kondo effect, is a well-known phenomenon that leads to anomalous transport measurements in bulk systems of dilute magnetic alloys.[21] For temperatures below the Kondo temperature (T_K), the electrons of the host screen the local spin of the impurity, and the result is the emergence of a Kondo resonance. This resonance should disappear at temperatures above T_K. A magnetic nanostructure comprising a magnetic impurity and a carbon nanotube host is an interesting system, since the impurity spins would interact with conduction electrons confined to one dimension and, in addition, might potentially spin-couple to a strongly (vs. weakly) interacting electron system.[22]

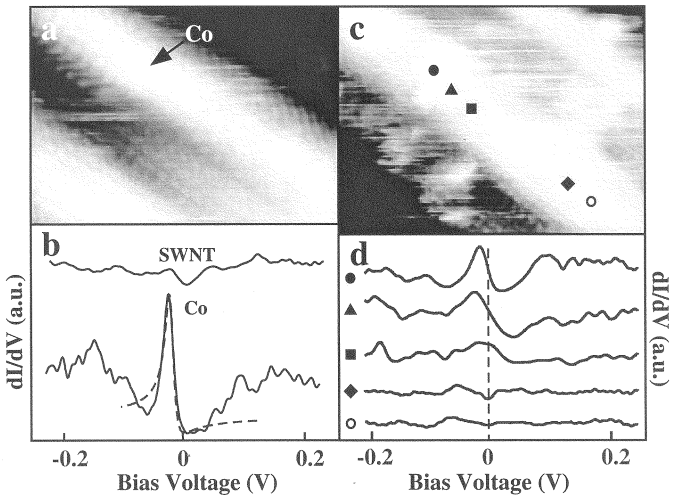

FIGURE 8. (a) STM image of 0.5-nm Co clusters situated on individual SWNTs. **(b)** Differential conductance, *dI/dV*, calculated from *I–V* curves taken over the bare nanotube ~7 nm away from the Co and above the Co cluster in part (a). The feature identified as a Kondo resonance appears over the Co. The *dashed line* indicates a fit to a theory explained in detail in Madhaven *et al.*[25] **(c)** STM image of slightly larger Co clusters <1 nm situated on resolved carbon nanotubes. (b) *dI/dV* as a function of position along the tube in part (a) (indicated by the symbols ●; ▲; ■; ◆; ○), starting with *I–V* performed over the cluster (●). The effect of the Co on the nanotube spectra is nearly gone after 2 nm. (Adapted from Odom *et al*.[23])

An STM image of individual SWNTs decorated with well-separated, 0.5-nm-diameter Co clusters is shown in FIGURE 8a. The spectroscopic data recorded on the bare nanotube ~7 nm away from the Co is finite and nearly constant over the small bias range, consistent with the nanotube being metallic (FIG. 8b). In contrast, the *dI/dV* spectrum taken directly above the Co center shows a strong resonance peak near E_F, $V = 0$. This spectroscopic feature was observed above 10 different small Co clusters (<1 nm) situated on metallic nanotubes and is strongly suggestive of the presence of a Kondo resonance in the 1D SWNTs.[23]

STM has the ability to resolve spatially the extent of local perturbations, and we took advantage of this capability to characterize the length scale over which the impurity inuences the nanotube's electronic spectrum. Spectroscopic data obtained for a 0.7-nm-wide Co cluster on an atomically resolved metallic SWNT (FIG. 8c) are shown in FIGURE 8d. At the center of the Co site, the resonance feature exhibits a peak structure similar in shape but slightly broader than the peak in FIGURE 8a. The peak feature systematically decreases in amplitude in spectra recorded at increasing distances from the Co center; the sharp resonance disappears completely after ~2 nm. This decay length is similar, although slightly longer than that reported for Co atoms on either Au(111) or Cu(111) surfaces.[24,25]

We have carried out a number of control experiments to verify that the prominent spectroscopic resonances are due to the interaction of the magnetic Co with the me-

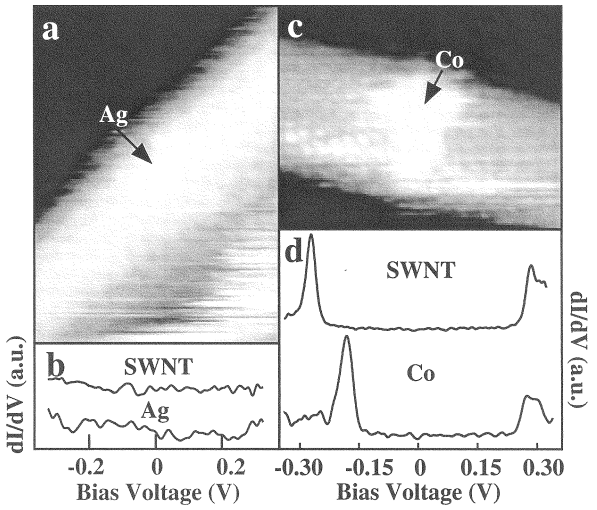

FIGURE 9. **(a)** Constant-current image of a small Ag cluster on an individual nanotube. **(b)** *dI/dV* taken over the Ag and bare nanotube 2 nm away. No features are observed in the spectra because of the presence of the Ag cluster. **(c)** Constant-current image of a Co cluster on a semiconducting nanotube. **(d)** *dI/ dV* taken above the Co and bare nanotube 5 nm away. The energy gap is slightly smaller over the Co, but there is no feature near E_F, indicating the necessity of conduction electrons at E_F of the host.

tallic SWNTs; that is, are indeed Kondo resonances. First, we repeated these measurements with nonmagnetic Ag clusters on SWNTs (FIG. 9a) and found no peak feature near E_F in the tunneling spectra due to the small Ag cluster (FIG. 9b). This result demonstrates unambiguously that the presence of the magnetic Co cluster is critical to observe the resonance and that the observed peak feature is not simply an enhancement in the local DOS as the result of a metallic cluster. Second, spectroscopic measurements performed over Co clusters supported by intrinsic semiconducting SWNTs exhibited no features at E_F (FIG. 9c,d). This observation suggests that the peak feature at E_F is not due to the bare Co *d*-orbital resonance and emphasizes the necessity of conduction electrons in the host needed to interact with the magnetic cluster in order to observe the Kondo resonance.

In addition, we have quantified our results for small Co clusters on metallic carbon nanotubes by fitting the observed spectroscopic features to a modified Anderson single-impurity model.[25] The dashed curve in FIGURE 8b shows a relatively good fit to the data taken above the center of the Co. The fit reveals that the Kondo temperature for the Co/SWNT system is ~90 K, confirming that the measurements at 5 K were made in the $T < T_K$ limit. To examine the validity of this prediction for T_K, we repeated our measurements at 80 K. Significantly, we found no peaks in *dI/dV* over Co sites situated on metallic SWNTs. We believe that this observation is consistent with the predicted value of T_K, although the disappearance occurs at a temperature approximately 10 K lower than obtained from the fit.

Perhaps the ultimate magnetic nanostructure is a magnetic atom in a quantum box. We are able to create such nanostructures by the cutting method described ear-

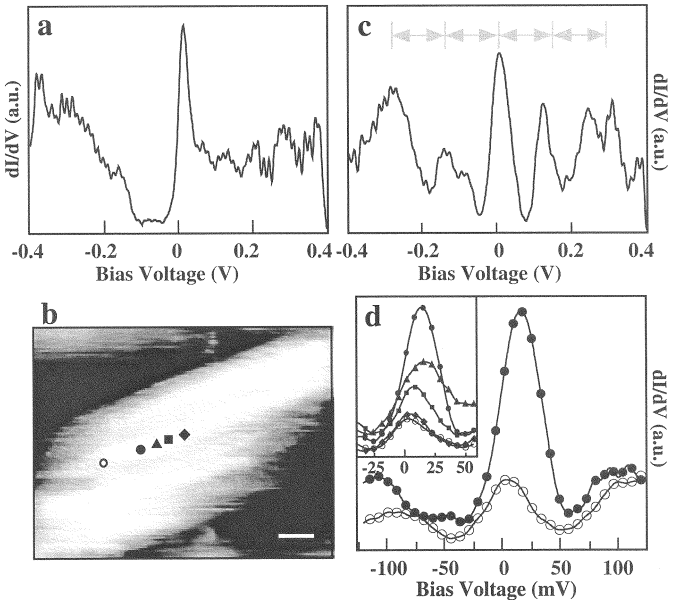

FIGURE 10. (a) *dI/dV* spectrum recorded at the site of a small Co cluster on a long nanotube. This same tube and Co site were probed in the data presented in parts (b) through (d). **(b)** Atomically resolved image of a nanotube shortened to 11 nm. The symbols ●; ▲; ■; ◆; ○ indicate the positions at which *I–V* curves were taken, and the *filled black circle* (●) highlights the position of the cluster. The *scale bar* corresponds to 1 nm. **(c)** *dI*/*dV* results obtained at the position of the small Co cluster in (b). The *gray arrows* indicate a near equidistant peak-splitting characteristic of the discrete energy-level spacing of an 11-nm nanotube quantum box. **(d)** Comparision of the peak amplitude near E_F recorded at the Co cluster (●) and about 1.5 nm away (○). *Inset*: *d/dV* data recorded at the positions indicated in (a). (Adapted from Odom *et al.*[23])

lier and have characterized Co on SWNTs spectroscopically before and after manipulating the nanotube length. The familiar Kondo resonance is observed near $V = 0$ in the *dI*/*dV* for spectra taken above a Co cluster situated on an uncut metallic SWNT (FIG. 10a). An atomically resolved 11-nm nanotube segment created by applying voltage pulses on each side of the Co cluster is shown in FIGURE 10b. Spectroscopic data recorded over the Co site (FIG. 10c) exhibit an average level spacing of ~0.15 eV, in agreement with the length-dependent level spacing discussed above. Notably, the peak amplitude at E_F appears enhanced significantly relative to the other energy level peaks. To investigate the origin of this increased conductance, we characterized the level structure near E_F versus distance from the cluster (FIG. 10d). The amplitude of this central peak at E_F decreases over the same length scale, 2 nm, as the Kondo resonance decays from a Co cluster along an extended 1D SWNT, although the amplitude of peaks at $E \neq E_F$ are similar. The enhanced conductance at E_F provides evidence of the sensitivity of the electronic properties of metallic nanotubes to magnetic impurities, even in finite-sized structures.

CONCLUSIONS

Our STM studies indicate that 1D SWNTs exhibit a richness in electronic behavior that may be exploited for molecular device applications. For example, metallic nanotubes may be used in resonant tunneling devices and also function as interconnects between device elements. Semiconducting nanotubes have already shown their utility in nanometer-sized field-effect transistors. Also, finite-sized SWNTs may be employed to raise the operating temperature of nanotube-based devices. Finally, metallic nanotubes decorated with magnetic impurities exhibit an enhancement in their conductance at low energies, and unique applications of these magnetic nanostructures may soon be uncovered.

REFERENCES

1. RUECKES, T. *et al*. 2000. Science **289:** 94.
2. TANS, S.J., R.M. VERSCHUEREN & C. DEKKER. 1998. Nature **393:** 49.
3. DEKKER, C. 1999. Phys. Today **52:** 22.
4. DUAN, X., Y. HUANG, Y. CUI & C.M. LIEBER. 2001. Nature **409:** 66.
5. CUI, Y. & C.M. LIEBER. 2001. Science **291:** 851–853.
6. LIEBER, C.M. 1998. Solid State Commun. **107:** 607.
7. HU, J.T., T.W. ODOM & C.M. LIEBER. 1999. Accts. Chem. Res. **32:** 435.
8. HAMADA, N., S. SAWADA & A. OSHIYAMA. 1992. Phys. Rev. Lett. **68:** 1579.
9. MINTMIRE, J.W., B.I. DUNLAP & C.T. WHITE. 1992. Phys. Rev. Lett. **68:** 631.
10. SAITO, R., M. FUJITA, G. DRESSELHAUS & M.S. DRESSELHAUS. 1992. Appl. Phys. Lett. **60:** 2204.
11. THESS, A. *et al*. 1996. Science **273:** 483.
12. WILDÖER, J.W.G. *et al*. 1998. Nature **391:** 59.
13. ODOM, T.W., J.-L. HUANG, P. KIM & C.M. LIEBER. 1998. Nature **391:** 62.
14. KIM, P., T.W. ODOM, J.-L. HUANG & C.M. LIEBER. 1999. Phys. Rev. Lett. **82:** 1225.
15. BLASÉ, X., L.X. BENEDICT, E.L. SHIRLEY & S.G. LOUIE. 1994. Phys. Rev. Lett. **72:** 1878.
16. ODOM, T.W., J.-L. HUANG, P. KIM & C.M. LIEBER. 2000. J. Phys. Chem. B **104:** 2794.
17. BOCKRATH, M. *et al*. 1997. Science **275:** 1922.
18. TANS, S.J. *et al*. 1997. Nature **386:** 474.
19. VENEMA, L.C. *et al*. 1997. Appl. Phys. Lett. **71:** 2629.
20. LIU, J. *et al*. 1998. Science **367:** 1253.
21. KONDO, J. 1964. Prog. Theor. Phys. **32:** 37.
22. BOCKRATH, M. *et al*. 1999. Nature **397:** 598.
23. ODOM, T.W., J.-L. HUANG, C.L. CHEUNG & C.M. LIEBER. 2000. Science **290:** 1549.
24. LI, J., W.-D. SCHNEIDER, R. BERNDT & B. DELLEY. 1998. Phys. Rev. Lett. **80:** 2893.
25. MADHAVAN, V. *et al.* 1998. Science **280:** 567.